ISSN 0016-7029, Geochemistry International, 2019, Vol. 57, No. 2, pp. 134–150. © Pleiades Publishing, Ltd., 2019.
Russian Text © Yu.A. Litvin, A.V. Spivak, 2019, published in Geokhimiya, 2019, No. 2.

Genesis of Diamonds and Paragenetic Inclusions under Lower Mantle Conditions: The Liquidus Structure of the Parental System at 26 GPa

Yu. A. Litvin[a], * and A. V. Spivak[a]

[a] *Korjinsky Institute of Experimental Mineralogy, Russian Academy of Sciences, Chernogolovka, 142432 Russia*
**e-mail: litvin@iem.ac.ru*

Received January 16, 2018; revised March 22, 2018; accepted April 6, 2018

Abstract—The regularities of the joint genesis of diamonds and their paragenetic inclusions under lower mantle conditions are controlled by the melting relations at the liquidus of the multicomponent diamond-forming system. The boundary compositions of this system are evident from the generalized data on the analytical mineralogy of paragenetic inclusions in lower-mantle diamonds. The structure of the liquidus of the diamond-forming system was studied in a physicochemical experiment for *P–T* parameters typical of the depths of 670–800 km. The compositions of parental melts/solutions for diamonds and paragenetic inclusions correspond to the multicomponent system MgO–FeO–CaO–SiO_2–$MgCO_3$–$FeCO_3$–$CaCO_3$–Na_2CO_3–C. Its primary melting is controlled by the peritectic phase relations at the solidus, which was shown as a result of experimental studies of polythermal sections of the system during a study of their phase diagrams. Of key importance is the effect of the "stishovite paradox," i.e., the peritectic reaction between the ultrabasic bridgmanite phase and melt with the formation of basic oxide associations of periclase–wustite solid solutions and stishovite. The peritectic reaction of bridgmanite is a fundamental feature of the diamond-forming system and determines the major peculiarity in its liquidus structure. Structure of the peritectic liquidus provides the physicochemical basis for the evolution of growth melts of diamonds and their paragenetic minerals. Based on the experimental data, we have constructed a fractional diagram of syngenesis of diamonds and inclusions clearly illustrating the solution–melt mechanism of diamond genesis and sequence of growth trapping of primary inclusions by diamonds under the lower-mantle conditions. The physicochemical factors of the genesis of diamonds and primary inclusions are agreed and generalized in a compositional diagram of lower-mantle diamond-forming media, and they provide a natural basis for the genetic classification of inclusions of rock-forming and accessory minerals in diamonds

Keywords: lower-mantle diamonds, primary mineral inclusions, parental melts/solutions, peritectic reaction of bridgmanite, stishovite paradox, fractional ultrabasic–basic evolution, genetic classification of inclusions, physicochemical experiment

DOI: 10.1134/S001670291902006X

INTRODUCTION

Experimental studies of subsolidus transformations in upper-mantle garnet lherzolite and their hypothetical "pyrolytic" analogs under the *P–T* lower-mantle conditions were based on the idea on the isochemical "pyrolite" composition of original rocks of the Earth's mantle over the entire depth range (Ringwood, 1975). Among the rock-forming minerals of ultrabasic rocks of the lower mantle are ferropericlase (Mg,Fe)O, bridgmanite (Mg,Fe)SiO_3, and Ca-perovskite $CaSiO_3$. Direct evaluation of the reliability of the experimental results is impossible, because rocks of the lower mantle were not found among deep xenoliths in kimberlite. However, kimberlite hosts rare samples of lower-mantle diamonds with primary inclusions of ferropericlase, bridgmanite, and Ca-perovskite (Scott Smith et al., 1984, Kaminsky et al., 2009; Bulanova et al., 2010). This indicates that kimberlite magmas transporting diamonds with primary inclusions formed at depths of the lower mantle. The genesis of diamonds with such inclusions in placers also corresponds to the *P–T* lower-mantle conditions (Harte and Harris, 1994; Kaminsky et al., 2000; Kaminsky, 2012).

According to the mantle carbonatite theory of diamond genesis (Litvin et al., 2016; Litvin, 2017), the primary paragenetic minerals of inclusions crystallized together with lower-mantle diamonds in the same multicomponent silicate–oxide–carbonate–carbon growth melt and were fragmentarily trapped by growing diamonds. Strictly speaking, the minerals of inclusions in diamonds have a genetic history different from that of the minerals from original lower-mantle rocks and, therefore, their direct identification is impossible. However, it is very likely that at the forma-

tion stage of diamond-forming media, original rocks of the lower mantle were first subjected to metasomatic carbonation and were then dissolved in newly formed primary carbonate melts (Litvin et al., 2014). These processes resulted in the formation of diamond-forming, completely miscible silicate–oxide–carbonate melts/carbon solutions . At the diamond genesis stage, the primarily dissolved components of original silicate and oxide minerals of the lower mantle could have crystallized from the parental medium as minerals similar to mantle ferropericlase, bridgmanite, Ca-perovskite, magnesiowustite, and stishovite. This allows us to indirectly correlate the minerals of paragenetic inclusions in diamonds with minerals of original rocks of the lower mantle. Thus, the experimental subsolidus data on the probable mineralogy of ultramafic lower-mantle rocks are additionally substantiated.

Both ultrabasic and basic minerals in association with stishovite were found among primary inclusions in lower-mantle diamonds (Kaminsky, 2012). Inclusions of ultrabasic and basic minerals were trapped by growing diamonds from a multiphase silicate–oxide–carbonate–carbon growth medium. This conclusion agrees with the strict requirements of the syngenesis criterion (Litvin, 2007), which should be consistent with any realistic version of the composition of the mantle diamond-forming medium. According to this criterion, diamonds and their paragenetic inclusions were formed and trapped in the same parental medium. Of special importance are inclusions of stishovite in the paragenesis with the phases of completely miscible periclase–wustite solid solutions. The paragenetic intergrowths of stishovite with ferropericlase/magnesiowustite and other lower-mantle minerals in inclusions provide unambiguous evidence for in situ genesis of stishovite under the lower-mantle conditions. Appearance of stishovite indicates probability of paragenetic transformations in the diamond-forming silicate–oxide–carbonate system of the lower mantle from the ultrabasic (ferropericlase + bridgmanite) mineral associations to the basic ones with magnesiowustite and stishovite. At the same time, we may expect such transitions in the original magmatic silicate–oxide systems of the lower mantle as well. In both cases, the ultrabasic–basic transitions should provide the clear typomorphic signs to "through" rock-forming minerals: the high concentrations of alumina in ferrobridgmanite $(Mg,Fe,Al)SiO_3$ and sodium in Ca-perovskite $(Ca,Na)SiO_3$, as it is registered in inclusions in diamonds.

The silicate–oxide system $MgO–FeO–SiO_2–CaSiO_3$ is rather representative for the ultrabasic and basic mineral associations of ferropericlase, bridgmanite, Ca-perovskite, stishovite, and magnesiowustite, which predominate in inclusions in diamonds and most likely in original rocks of the lower mantle. The melting relations in the polythermal section $(MgO)_{70}(FeO)_{30}–(SiO_2)_{70}(FeO)_{30}$ of the boundary $MgO–FeO–SiO_2$ system were studied at 24 GPa (Litvin et al., 2016a, 2016b, 2017). It was shown that ferrobridgmanite $(Mg,Fe)SiO_3$ was decomposed in the peritectic reaction with the melt, resulting in the formation of an association of stishovite with the phases of periclase–wustite solid solutions. This reaction was predicted theoretically as the "stishovite paradox" (Litvin, 2014). Such an effect can be also expected in the $MgO–FeO–SiO_2–CaSiO_3$ system, in which the lower-mantle association of ultrabasic and basic rocks is fully represented. This may be also related to the multicomponent silicate–oxide–carbonate–carbon system, which includes the parental medium of diamonds and their paragenetic inclusions under lower-mantle conditions.

This study is aimed at physicochemical experimental (26 GPa) and theoretical studies of (1) the peritectic effect of the stishovite paradox in lower-mantle systems of both parental material $MgO–FeO–SiO_2–CaSiO_3$ and the diamond-forming medium $MgO–FeO–SiO_2–CaSiO_3$–(Mg–Fe–Ca–Na-carbonate)–C; (2) the role of the physicochemical mechanism of the stishovite paradox in the ultrabasic–basic evolution of parent lower-mantle silicate–oxide magmas, as well as silicate–oxide–carbonate–carbon melts and solutions parental for diamonds and minerals genetically associated with them. The expected experimental results and conclusions are of special interest as the basis for a generalized diagram of the compositions of lower-mantle parental media of diamonds and primary inclusions.

EXPERIMENTAL, THEORETICAL, AND ANALYTICAL METHODS

The liquidus melt relations in the lower-mantle parental silicate–oxide and diamond-forming silicate–oxide–carbonate ± carbon systems were studied experimentally at 26 GPa on a multianvil apparatus (Frost et al., 2004) at the Bayerisches Geoinstitute, University of Bayreuth. The starting materials included powders of oxides (MgO, FeO, CaO, and SiO_2), carbonates ($MgCO_3$, $FeCO_3$, $CaCO_3$, and Na_2CO_3), and ultrapure graphite. The errors in pressure and temperature estimation were within 0.5–1.0 GPa and ±50°C, respectively. Experimental studies of lower-mantle systems with complex compositions are probable only in combination with the theoretical methods of physical chemistry of multicomponent multiphase systems (Rhines, 1956; Palatnik and Landau, 1964; Zakharov, 1964). This is necessary due to application of the concept of the phase complex, methods of simplex triangulation of diagrams, coordinate transformation, two-dimensional polythermal sections, the Rhines–Palatnik–Landau phase rule, etc. Polythermal sections as representative two-dimensional projections provide clear evidence for the key physicochemical transformations of multicomponent lower-

mantle systems. The topological reliability of the phase diagrams can be tested using the Rhines–Palatnik–Landau phase rule. Multiphase experimental samples and their compositions were studied on a CamScan M2300 SEM (VEGA TS 5130M)–Link INCA energy-dispersive microprobe at the Institute of Experimental Mineralogy, Russian Academy of Sciences (Chernogolovka, Moscow oblast).

EXPERIMENTAL STUDIES OF MULTICOMPONENT SYSTEMS OF THE PARENT AND DIAMOND-FORMING MATERIAL OF THE LOWER MANTLE

Most likely, the formation of parental melts and solutions for lower-mantle diamonds, as well as for minerals genetically associated with them, occurred in ultrabasic silicate–oxide rocks as a result of successive metasomatic and magmatic processes (Litvin et al., 2014). First, the reactions of carbon dioxide alkaline metasomatic agents with lower-mantle rocks could have resulted in the formation of carbonate melts (Litvin, 1998). Later, carbonate melts dissolved rock-forming and accessory minerals of the lower mantle, forming completely miscible silicate–oxide–carbonate melts with dissolved elementary carbon. Under diamond formation conditions, dissolved silicate, oxide, and carbonate components of parental melts could have crystallized again as minerals similar to the parent minerals of the lower mantle. As evident from the experimental studies, the physicochemical peritectic mechanism, determined as an effect of the stishovite paradox (Litvin, 2014),is typical of magmatic silicate–oxide and diamond-forming silicate–oxide–carbonate melts of the lower mantle.

Melting relations in systems of lower-mantle parent material. The typical mineral associations, including ultrabasic (ferropericlase [*FPer* = $(MgO \cdot FeO)_{ss}$] + ferrobridgmanite [*FBrd* = $(Mg,Fe)SiO_3$] + Ca-perovskite [*CaPrv* = $CaSiO_3$]) and basic (magnesiowustite [*MWus* = $(FeO \cdot MgO)_{ss}$] + stishovite [*Sti* = SiO_2]), belong to the system $MgO–FeO–SiO_2–CaSiO_3$. It should be emphasized that *FPer* and *MWus* are the phases of complete periclase–wustite solid solutions $(Per \cdot Wus)_{ss}$. The melting relations in the polythermal section $(MgO)_{49}(FeO)_{21}(CaSiO_3)_{30}–(SiO_2)_{49}(FeO)_{21}(CaSiO_3)_{30}$ of this system at 26 GPa (Table 1, Figs. 1 and 2) illustrate the peritectic interaction of ferrobridgmanite, resulting in the formation of a basic association of stishovite and magnesiowustite. In this case, the peritectic association (*P*) includes *L* + *FBrd* + *MWus* + Ca-perovskite *CaPrv* + stishovite *Sti*; the key reaction *L* + *FBrd* = *Sti* + *MWus* results in loss of *FBrd* (an effect of the stishovite paradox). The liquidus associations on the experimental phase diagram (Fig. 1) are *L* + *FPer* and *L* + *Sti*, *L* + *FPer* + *FBrd* (Fig. 2a) and *L* + *FPer* + *FBrd* + *CaPrv*, as well as *L* + *MWus* + *Sti* (Fig. 2b). The solidus associations, including *L* + *FBrd* + *MWus* + *Sti* + *CaPrv* and *L* + *MWus* + *Sti* + *CaPrv*, illustrate the disappearance of ferrobridgmanite as a result of the peritectic reaction (*P*). Among the stable subsolidus associations are *FPer* + *FBrd* + *CaPrv* (Fig. 2c), *Fbrd* + *MWus* + *Sti* + *CaPrv* (Fig. 2d) and *MWus* + *Sti* + *CaPrv*.

The physicochemical experimental results and conclusions are in full compliance with preliminary estimates (Litvin et al., 2016a, 2016b) of the liquidus structure of the system $MgO–FeO–SiO_2–CaSiO_3$ modeling the parental material of the lower mantle (Fig. 3). The eutectic e_1 of the boundary system *Per–Brd–CaPrv* controls melting of low-Fe rocks of the lower mantle and generation of the primary ultrabasic magma. With decreasing temperature, the composition of magma should change along the monovariant cotectic *L* + *FPer* + *FBrd* + *CaPrv* ("*a*") to the peritectic point *L* + *FBrd* + *MWus* + *Sti* + *CaPrv* ("*P*"), in which *FBrd* disappears due to the reaction of the stishovite paradox. With a further decrease in temperature, this results in the formation of the monovariant cotectic *L* + *MWus* + *Sti* + *CaPrv* ("c") and, accordingly, the eutectic e_3 in the boundary system *Wus–Sti–CaPrv*. It is necessary to emphasize the key role of the peritectic reaction of the stishovite paradox as the physicochemical mechanism allowing the ultrabasic–basic evolution of lower-mantle magmatism.

However, the effective ultrabasic–basic evolution of lower-mantle magmas may proceed only in the mode of their fractional crystallization. This provides continuous fractional removal of newly formed minerals from magmatic melts with decreasing temperature, which is accompanied by a balanced change in the composition of residual melts. Such continuous renewal of the composition of residual melts modifies the general composition of fractionating petrological system from the beginning to the end and controls its intermediate compositions (in the idealized approximation). Thus, fractional crystallization may stimulate a gradual transition from ultrabasic to basic minerals under the lower-mantle conditions. The ultrabasic–basic evolution of parental material of the lower mantle is impossible under the conditions of equilibrium melting and crystallization of the corresponding petrological systems, when the starting and final compositions of the crystallizing system should be the same.

Melting relations in parental lower-mantle systems for diamonds and primary inclusions. The primary inclusions in lower-mantle diamonds are represented by ultrabasic (ferropericlase, ferrobridgmanite, Ca-perovskite) and basic (magnesiowustite, stishovite) minerals; in addition, ferrobridgmanite Ca-perovskite with typomorphic high concentrations of Al and Na, respectively, should also be referred to basic minerals. The minerals of both ultrabasic and basic inclusions are associated with Mg, Fe, Ca, and Na carbonates, whereas K carbonates abundant among primary inclusions in upper-mantle diamonds (Schrauder and

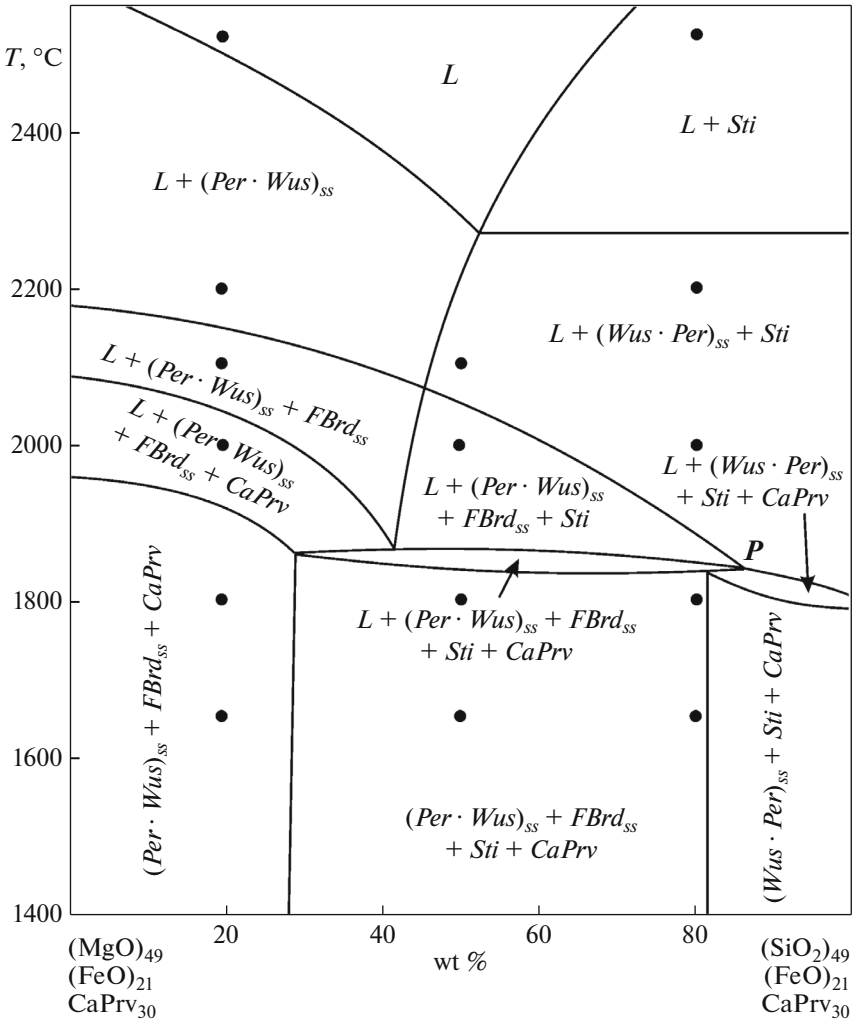

Fig. 1. Melting relations in the polythermal section $(MgO)_{49}(FeO)_{21}(CaSiO_3)_{30}$–$(SiO_2)_{49}(FeO)_{21}(CaSiO_3)_{30}$ at 26 GPa. The run conditions are indicated by black spots. *L*, melt; *Per*, periclase; *Wus*, wustite; *FPer*, ferropericlase; *MWus*, magnesiowustite; *FBrd*, ferrobridgmanite; *CaPrv*, Ca-perovskite; *Sti*, stishovite; quasi-nonvariant peritectic point $L + FBrd + [(Per \cdot Wus)_{ss} \leftrightarrow (Wus \cdot Per)_{ss}] + Sti + CaPrv$ with the key reaction $L + FBrd = Sti + (Wus \cdot Per)_{ss}$ of the stishovite paradox.

Navon, 1994; Zedgenizov et al., 2011; Skuzovatov et al., 2012) are not typical of lower-mantle diamonds (Kaminsky, 2012). Lower-mantle diamond-forming melts/solutions mostly belong to the silicate–oxide–carbonate–carbon system MgO–FeO–CaO–SiO_2–(Mg–Fe–Ca–Na-carbonate)–C (Litvin et al., 2014), with account for mutually consistent results of physicochemical experiments and analytical mineralogy of inclusions. Experimental studies up to 26 GPa provided evidence for incongruent melting in the Mg–Fe–Ca–Na-carbonate system with completely miscible multicomponent carbonate melts, which are stable in a wide range of pressures and temperatures (Spivak et al., 2015). All these facts allow us to consider the mineral composition of primary inclusions in lower-mantle diamonds within the experimental system MgO–FeO–CaO–SiO_2–*Carb**–C, where *Carb** denotes both the starting carbonate composition $(MgCO_3)_{25}(FeCO_3)_{25}(CaCO_3)_{25}(Na_2CO_3)_{25}$ and entire set of subsolidus phases $(Mg,Fe)CO_3$ + $(Ca,Na_2,Fe,Mg)CO_3$ + $Na_2(Ca,Fe,Mg)(CO_3)_2$ (Spivak et al, 2015). This remarkably simplifies the phase diagrams using the generalized symbol *Carb** and one phase field instead of three separate phase fields in each case. Participation of the carbonate component in the multicomponent composition of the silicate–oxide–carbonate–carbon diamond-forming system promotes complete miscibility of silicate–oxide–carbonate melts; high solubility of ultramafic and mafic minerals, as well as diamond and graphite in these melts; and efficient diffusive transport of carbon dissolved in melts, as well as lower melting temperatures of the diamond-forming multicomponent compositions in relation to the geothermal values. As a result, diamond-forming melts and solutions are formed, and they are the basis for the mantle carbonatite theory of

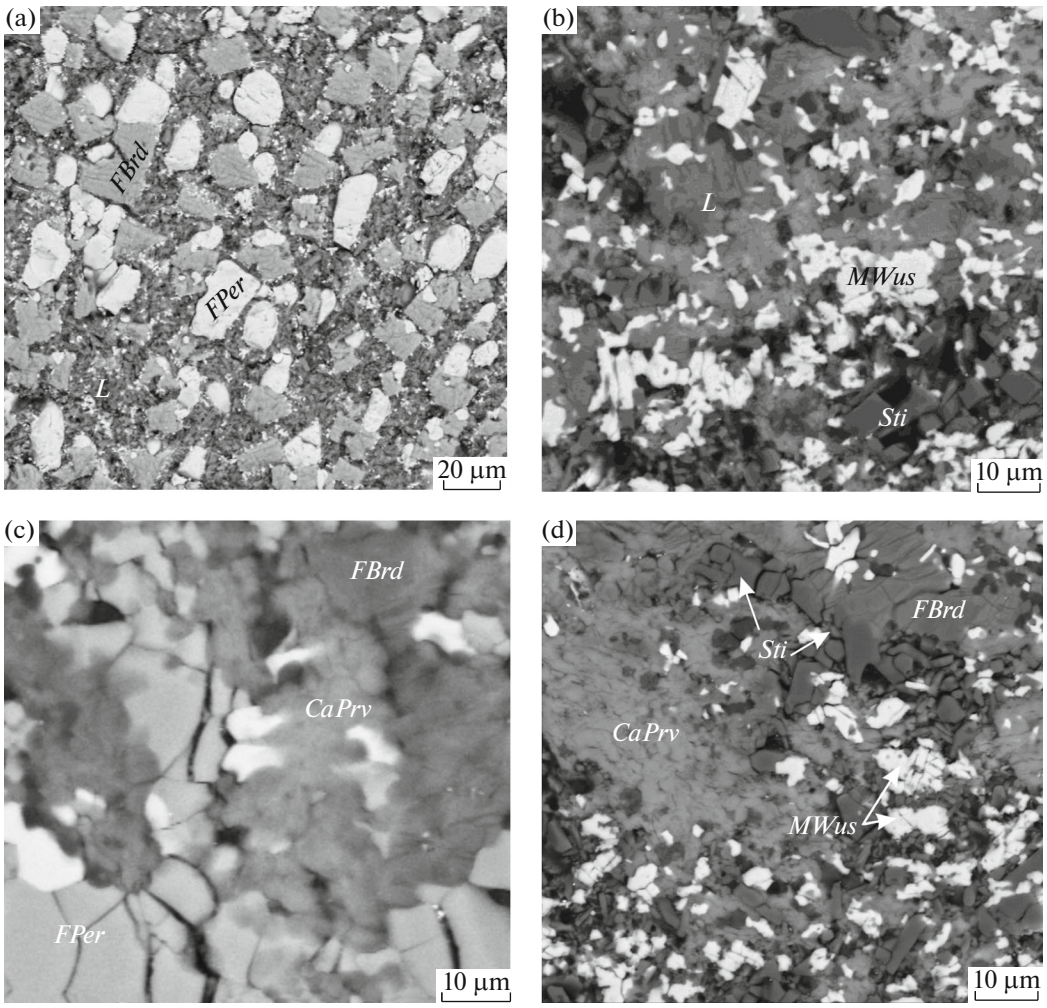

Fig. 2. SEM images of experimental samples in the polythermal section $(MgO)_{49}(FeO)_{21}(CaSiO_3)_{30}$–$(SiO_2)_{49}(FeO)_{21}(CaSiO_3)_{30}$ at 26 GPa after quenching. The starting compositions: (a, c) $(MgO)_{39.2}(FeO)_{21}(SiO_2)_{9.8}(CaSiO_3)_{30}$; (b) $(MgO)_{24.5}(FeO)_{21}(SiO_2)_{24.5}(CaSiO_3)_{30}$; (d) $(SiO_2)_{39.2}(FeO)_{21}(MgO)_{9.8}(CaSiO_3)_{30}$. *FPer*, ferropericlase [= $(Per \cdot Wus)_{ss}$]; *MWus*, magnesiowustite [= $(Wus \cdot Per)_{ss}$]. See Fig. 1 for other mineral symbols.

the origin of diamonds and associated phases (Litvin et al., 2016; Litvin, 2017).

Our experimental studies demonstrate melting relations in the diamond-forming system at 26 GPa in the polythermal sections $(MgO)_{30}(FeO)_{20}Carb^*_{50}$–$(SiO_2)_{30}(FeO)_{20}Carb^*_{50}$ without *CaPrv* (Figs. 4 and 5, Table 2), as well as $(MgO)_{20}(FeO)_{15}(CaSiO_3)_{15}Carb^*_{50}$–$(SiO_2)_{20}(FeO)_{15}(CaSiO_3)_{15}Carb^*_{50}$ with *CaPrv* (Figs. 6 and 7, Table 3). It is very important that in both cases we observe peritectic interaction of ferrobridgmanite with carbonate-bearing melts with the formation of a basic association of stishovite, magnesiowustite, and carbonates. In the latter case (Fig. 6), the quasi-nonvariant peritectic point *P* corresponds to the association of $L + FBrd + (MWus/FPer)_{ss} + CaPrv + Sti + Carb^*$ with the key reaction between carbonate-bearing melt and bridgmanite $L + FBrd = Sti + (MWus/FPer)_{ss} + Carb^*$ with loss of *FBrd* (an effect of the stishovite paradox). In the phase diagrams of the studied polythermal sections, both liquidus phases *FPer*, *Sti* and subliquidus associations, as well as subsolidus parageneses $FPer + FBrd + Carb^* \pm CaPrv$ and $FBrd + (MWus/FPer)_{ss} + Sti + Carb^* \pm CaPrv$ show the ultrabasic–basic evolution in the melting relations. Experiments on crystallization of diamonds and associated paragenetic minerals at 1700°C in common parental melts and solutions of the carbon-bearing system $(MgO)_{30}(FeO)_{20}Carb^*_{50}$–$(SiO_2)_{30}(FeO)_{20}Carb^*_{50}$–C demonstrate the ultrabasic–basic transition in associations of minerals from inclusions in lower-mantle diamonds (Fig. 8). The experimental results obtained agree with the criterion of syngenesis, due to the ability of the parental medium to simultaneously form

Table 1. Run conditions, compositions of experimental phases, and estimates of the equilibrium mineral associations in the polythermal section $(MgO)_{49}(FeO)_{21}(CaSiO)_{30}$–$(SiO_2)_{49}(FeO)_{21}(CaSiO)_{30}$ of the original lower-mantle system MgO–FeO–SiO_2–$CaSiO_3$ at 26 GPa

Sample	T, °C	t, min	Experimental results						
			Phase association	Phase	MgO	FeO	SiO_2	CaO	Total
				wt %					
$(MgO)_{39.2}(SiO_2)_{9.8}(FeO)_{21}(CaSiO_3)_{30}$									
H4074-1a	2500	5	*L*	*L*	32.31	27.88	28.53	10.62	99.34
H4060a	2200	10	$L + (Per/Wus)_{ss}$	*L*	20.79	27.16	32.78	19.13	99.87
				FPer	64.38	34.51	0.49	0.48	99.80
H4065a	2100	10	$L + (Per/Wus)_{ss} + FBrd$	*L*	22.24	21.47	21.00	35.22	99.92
				MWus	43.06	55.61	0.28	0.34	99.29
				FBrd	33.19	11.86	54.38	0.54	99.97
H4070-1c	2000	20	$L + (Per/Wus)_{ss} + FBrd + CaPrv$	*L*	32.50	34.66	9.26	23.26	99.67
				MWus	42.89	56.22	0.16	0.59	99.86
				FBrd	35.79	6.28	57.37	0.42	99.83
				CaPrv	0.67	0.93	50.50	47.84	99.95
H4072-1a	1800	30	$(Per/Wus)_{ss} + FBrd + CaPrv$	*MWus*	43.55	55.04	0.49	0.31	99.39
				FBrd	34.86	7.70	56.83	0.38	99.76
				MWus	9.39	88.51	1.04	0.51	99.52
				CaPrv	0.49	0.66	49.37	48.80	99.32
H4073-1c	1650	30	$(Per/Wus)_{ss} + FBrd + CaPrv$	*FBrd*	31.70	10.08	55.26	2.84	99.88
				MWus	11.70	86.73	0.81	0.69	99.93
				CaPrv	0.52	0.63	55.52	47.96	99.62
$(MgO)_{24.5}(SiO_2)_{24.5}(FeO)_{21}(CaSiO_3)_{30}$									
H4073-1b	2200	5	*L*	*L*	19.86	25.88	40.85	13.09	99.68
H4065b	2100	10	$L + (Wus/Per)_{ss} + Sti$	*L*	29.66	13.64	27.62	29.01	99.94
				MWus	19.83	79.47	0.48	0.05	99.83
				Sti	0.29	0.72	98.91	–	99.92
H4070-1c	2000	20	$L + (Wus/Per)_{ss} + FBrd + Sti$	*L*	28.40	7.22	6.71	57.51	99.83
				MWus	11.55	86.63	1.30	0.45	99.93
				FBrd	32.88	11.23	55.47	0.32	99.90
				Sti	0.17	0.18	99.96	0.12	100.43
H4073-1b	1650	30	$(Wus/Per)_{ss} + FBrd + Sti + CaPrv$	*MWus*	8.57	88.03	2.11	0.91	99.61
				FBrd	33.29	8.05	58.04	1.09	100.47
				Sti	0.01	0.48	98.94	0.18	99.61
				CaPrv	1.53	0.91	49.11	48.25	99.80
$(MgO)_{9.8}(SiO_2)_{39.2}(FeO)_{21}(CaSiO_3)_{30}$									
H4074-1c	2500	5	$L + Sti$	*L*	9.91	30.51	41.26	17.99	99.67
				Sti	0.05	1.89	97.60	0.52	100.06
H4060c	2200	10	$L + Sti + (Wus/Per)_{ss}$	*L*	10.25	4.97	56.12	28.45	99.78
				Sti	–	2.13	97.14	0.72	99.99
				MWus	11.29	86.97	0.91	0.49	99.65
H4070-1c	2000	20	$L + Sti + (Wus/Per)_{ss}$	*L*	14.33	8.68	42.33	34.50	99.83
				Sti	–	0.48	98.92	0.08	99.48
				MWus	7.86	83.89	0.98	0.39	93.62
H4073-1a	1650	30	$(Wus/Per)_{ss} + FBrd + Sti + CaPrv$	*FBrd*	31.81	12.33	55.46	0.18	99.78
				MWus	8.58	88.35	2.06	0.66	99.66
				Sti	0.06	0.81	98.93	0.69	100.49
				CaPrv	0.21	1.91	49.61	47.77	99.50

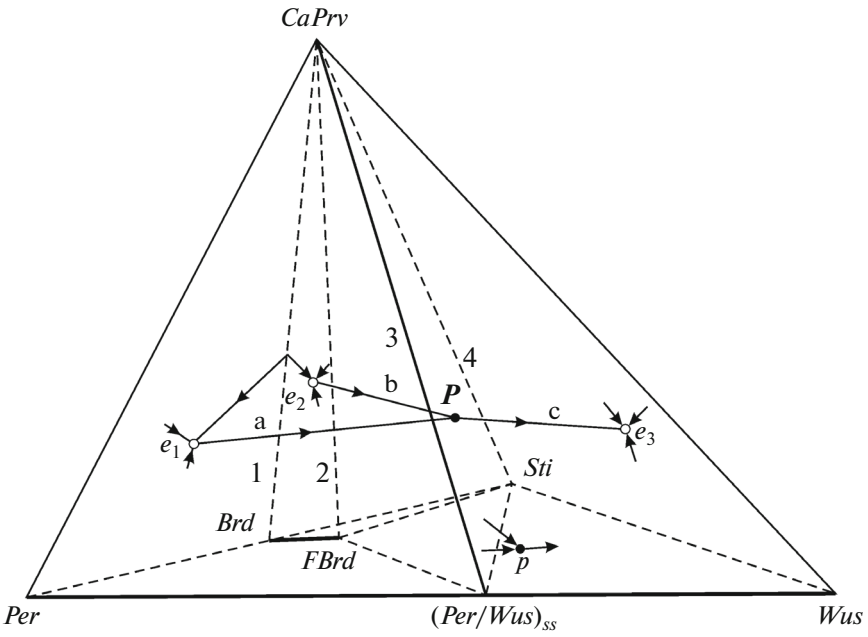

Fig. 3. Liquidus structure for the original lower-mantle system *Per–Wus–Sti–CaPrv* at 26 GPa. *Brd*, bridgmanite. See Figs. 1 and 2 for other phase symbols. Subsolidus triangular phase volumes are indicated as (1–4); eutectic and peritectic points of the ternary boundary systems, as e_1 (*L* + *Per* + *Brd* + *CaPrv*), e_2 (*L* + *Brd* + *Sti* + *CaPrv*), e_3 (*L* + *Sti* + *Wus* + *CaPrv*), and *p* (*L* + *Brd* = *Sti* + *MWus*); *P* is the quasi-nonvariant peritectic point *L* + (*FPer* ↔ *MWus*) + *FBrd* + *Sti* + *CaPrv* of the four-component system with the key reaction *L* + *FBrd* = *Sti* + (*Wus* · *Per*)*ss* of the stishovite paradox; monovariant cotectic curves: (a) ultrabasic *L* + *FPer* + *FBrd* + *CaPrv*; (b) basic *L* + *Sti* + *FBrd* + *CaPrv*; (c) basic *L* + *Sti* + *MWus* + *CaPrv*.

diamonds and minerals known as primary inclusions in natural diamonds.

FRACTIONAL CRYSTALLIZATION IN PARENTAL LOWER-MANTLE SYSTEMS FOR DIAMONDS AND PRIMARY INCLUSIONS

The results of experimental studies of melting relations in the most representative polythermal section $(MgO)_{20}(FeO)_{15}(CaSiO_3)_{15}Carb^*_{50}$–$(SiO_2)_{20}(FeO)_{15}(CaSiO_3)_{15}Carb^*_{50}$ (Fig. 6) of the diamond-forming system *Per–Wus–Sti–CaPrv–Carb**–C of the lower mantle provide evidence for the reliability of the structure of its basic silicate–oxide–carbonate liquidus (Fig. 9), preliminarily studied by Litvin et al. (2016b). This is significant in terms of genetic relation, since only elements of the liquidus structure can control the regular ultrabasic–basic evolution of parental melts and solutions for diamonds and primary inclusions. The diagram of the compositions of the multicomponent diamond-forming system (Fig. 9) is a complex consisting of one ultrabasic simplex (*Per,Carb**)–(*Brd,Carb**)–[(*Per/Wus*)$_{ss}$,*Carb**]–(*CaPrv,Carb**) (1) and three basic simplexes (*Sti,Carb**)–(*Brd,Carb**)–(*FBrd,Carb**)–(*CaPrv,Carb**) (2), (*Sti,Carb**)–(*FBrd,Carb**)–[(*Per/Wus*)$_{ss}$,*Carb**]–(*CaPrv,Carb**) (3), and (*Sti,Carb**)–[(*Per/Wus*)$_{ss}$,*Carb**]–(*Wus,Carb**)–(*CaPrv,Carb**) (4). A continuous physicochemical link between ultrabasic and basic melts can be attained only in the mode of fractional crystallization of minerals with decreasing temperature, when the figurative points of primary ultrabasic compositions (eutectic e_1 in the limiting case) move along the ultrabasic monovariant curve *L* + *FPer* + *FBrd* + *CaPrv* + *Carb** (a) towards the nonvariant peritectic *L* + *FBrd* + *CaPrv* + (*Per/Wus*)$_{ss}$ + *Sti* + *Carb** (*P*); after loss of *FBrd*, towards the basic monovariant curve *L* + (*Wus/Per*)$_{ss}$ + *Sti* + *CaPrv* + *Carb** (c). The key role is played by physicochemical mechanism of the stishovite paradox *FBrd* + *L* → *Sti* + (*Wus/Per*)$_{ss}$ + *Carb**.

The data of the physicochemical experiment obtained in this study support the topological reliability of the lower-mantle fractional diagram of syngenesis of diamonds and paragenetic mineral phases plotted in the plane of the polythermal section *FPer, FBrd, CaPrv, Carb**[→ *MWus,Sti,CaPrv,Carb**]–*D* (Fig. 10) and considered preliminarily in (Litvin et al., 2016b). In this case, paragenetic mineral inclusions may comprise not only primary mineral inclusions, but also rock-forming and accessory minerals of ultrabasic and basic diamond-bearing rocks of the lower mantle. The fractional diagram of syngenesis of diamonds and associated phases is differs fundamentally from the diagrams of syngenesis in an equilibrium approximation considered, e.g., by Litvin et al. (2016b), since its bulk composition is not fixed but varies in the course of crystallization. This feature required special abbre-

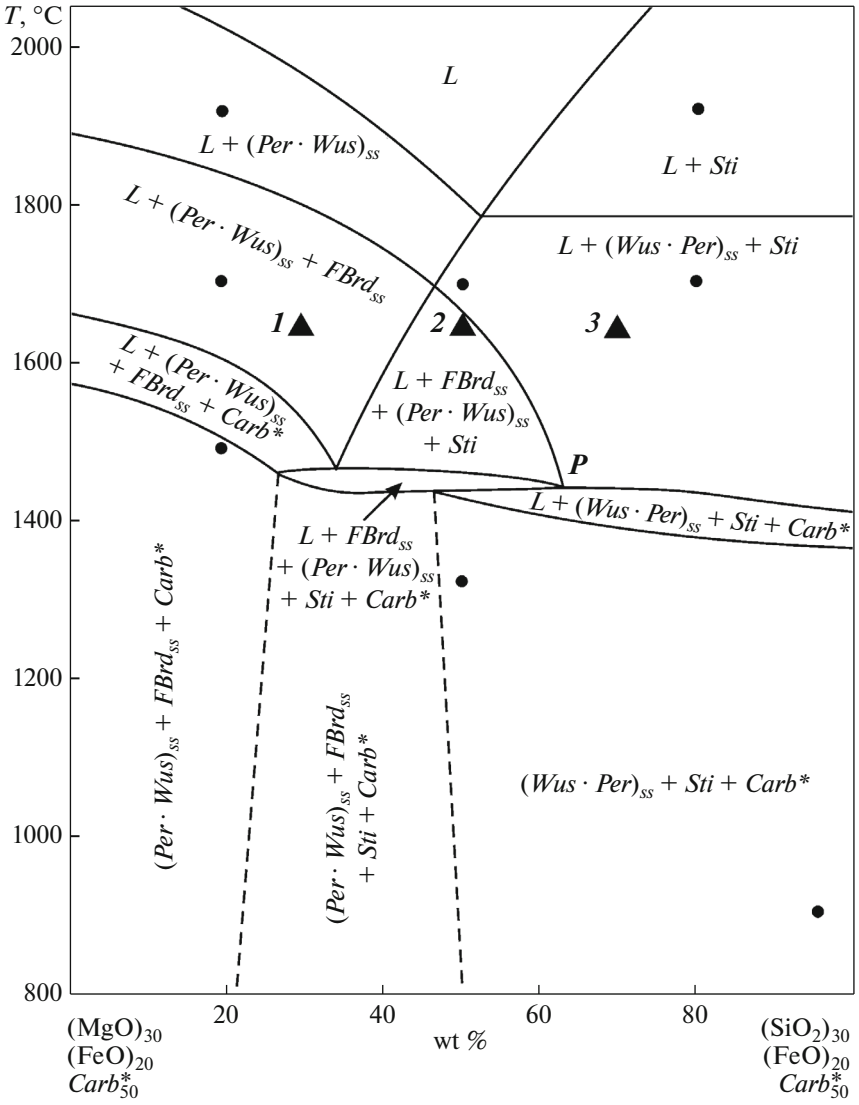

Fig. 4. Melting relations in the polythermal section $(MgO)_{30}(FeO)_{20}Carb^*_{50}$–$(SiO_2)_{30}(FeO)_{20}Carb^*_{50}$ at 26 GPa. *Carb**, simplified abbreviation for carbonates (explained in the text). See Fig. 1 for other mineral symbols.

viations for the polythermal section of the fractional diagram of syngenesis (Fig. 10): the primary ultrabasic mineral composition *FPer*, *FBrd*, *CaPrv*, *Carb** undergoes continuous variations in the course of fractional crystallization, shown by an arrow, up to the final basic mineral composition *MWus*, *Sti*, *CaPrv*, *Carb**, shown in square brackets.

The fractional diagram of syngenesis of diamonds and associated phases of the ultrabasic and basic parageneses (Fig. 10) includes the P–T–N_c diamond solubility curve; in this case P is constant, whereas the temperature T and carbon concentration N_c are variables. The solubility curve crosses areas of complete and partial melting in the syngenesis diagram. The diamond solubility curve reflects the phase states of completely miscible silicate–oxide–carbonate melts saturated with dissolved carbon with respect to diamond. A peculiar feature of the fractional crystallization mode is that the compositions of silicate–oxide–carbonate solvents of carbon evolve from ultrabasic to basic with decreasing temperature. Therefore, the diamond solubility curve should occupy a certain position in the compositional volume of this system, whereas in the polythermal section, it is shown in projection. The fractional phase diagram is divided by the diamond solubility curve into the compositional areas undersaturated in dissolved carbon (left) and saturated in relation to diamond (right). The key function of the solubility curve is reflected in realization of the diamond-forming process (Litvin, 2017). The physicochemical control shows that with decreasing temperature the figurative point of any composition of

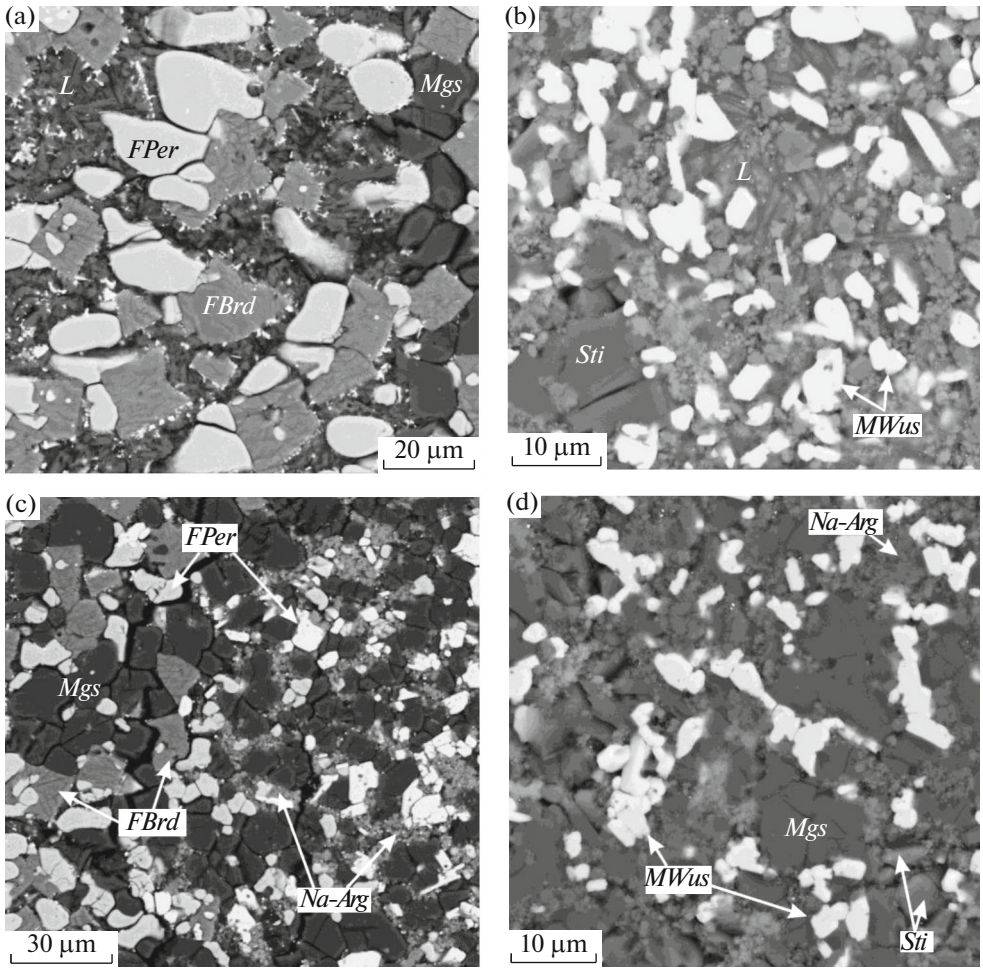

Fig. 5. SEM images of experimental samples in the polythermal section $(MgO)_{30}(FeO)_{20}Carb^*_{50}$–$(SiO_2)_{30}(FeO)_{20}Carb^*_{50}$ at 26 GPa after quenching. The starting compositions: (a, c) $(MgO)_{24}(FeO)_{20}(SiO_2)_6Carb^*_{50}$; (b, d) $(MgO)_{15}(FeO)_{20}(SiO_2)_{15}Carb^*_{50}$. *Carb**, simplified abbreviation for carbonates (explained in the text); *FPer*, ferropericlase [=$(Per \cdot Wus)_{ss}$]; *MWus*, magnesiowustite [= $(Wus \cdot Per)_{ss}$]; Na-*Arg*, Na-bearing aragonite. See Fig. 1 for other mineral symbols.

melt/solution saturated with carbon in relation to diamond plots beyond the solubility curve. As this takes place, the melt/solution automatically becomes oversaturated with respect to diamond. Nucleation of diamond is due to the achievement of a critical, in this case, "labile" supersaturation to diamond. Further growth of diamond crystals may be supported at levels of "metastable" supersaturation as well. Such processes of nucleation and growth of diamond crystals can be realized with a decrease in temperature to complete the solidification of silicate–oxide–carbonate–carbon solutions. The syngenesis diagram shows that with decreasing temperature, the figurative point of compositions of diamond-forming melts and solutions should pass through the phase fields of paragenetic mineral phases, which may be fragmentarily trapped by growing diamonds with the formation of primary inclusions. We can certify that the formation of basic minerals and their trapping by diamonds becomes possible only after the figurative point of the composition of diamond-forming melt/solution passes the peritectic losses ferrobridgmanite as a result of the effect of the stishovite paradox.

All genetically important materials involved in the lower-mantle genesis of diamonds and associated phases are summarized in the generalized diagram of the composition of parental diamond-forming media (Fig. 11). Consistence of the data of analytical mineralogy of primary inclusions in lower-mantle diamonds and the results of physicochemical experiments allows us to attribute lower-mantle diamond-forming media to a multicomponent multiphase system: (rock-forming minerals of the ultrabasic association)–(rock-forming minerals of the basic association)–(carbonate phases)–(admixture accessory minerals soluble in parental melts)–(admixture accessory minerals insoluble in parental melts)–carbon. The key role in the genesis of diamonds is played by the rock-forming

Table 2. Run conditions, compositions of experimental phases, and estimates of the equilibrium mineral associations in the polythermal section $(MgO)_{30}(FeO)_{20}Carb^*_{50}$–$(SiO_2)_{30}(FeO)_{20}Carb^*_{50}$ of the original lower-mantle system MgO–FeO–SiO_2–*Carb** at 26 GPa

Sample	*T*, °C	*t*, min	Experimental results								
			phase association	phase	MgO	FeO	SiO_2	CaO	Na_2O	CO_2^{**}	total
					wt %						
$(MgO)_{24}(SiO_2)_6(FeO)_{20}Carb^*_{50}$											
S6028-2	1900	30	$L + (Per/Wus)_{ss}$	*L*	18.89	23.13	9.21	9.67	8.39	30.71	100.00
				FPer	56.28	40.46	0.11	0.35	2.67	–	99.87
S6027-2	1700	30	$L + (Per/Wus)_{ss}$ + *FBrd*	*L*	26.41	12.23	6.83	14.15	18.32	22.06	100.00
				MWus	28.98	63.01	0.03	0.22	6.69	–	98.93
				FBrd	32.73	10.50	54.97	0.72	0.96	–	99.87
H3943-1	1500	60	$L + (Per/Wus)_{ss}$ + *FBrd* + *Carb**	*L*	25.83	5.49	5.20	17.26	14.55	31.67	100.00
				MWus	28.28	67.18	0.18	0.15	3.81	–	99.28
				MWus	7.51	81.59	0.68	0.48	0.32	–	90.59
				FBrd	33.46	10.64	54.57	0.31	0.45	–	99.43
				Mgs	45.00	6.15	0.10	0.42	0.55	47.78	100.00
H3944-1	900	120	$(Per/Wus)_{ss}$ + *FBrd* + *Sti* + *Carb**	*MWus*	27.67	67.69	0.05	0.01	3.93	–	99.51
				MWus	7.50	83.67	0.16	0.35	0.44	–	92.08
				Mgs	47.33	2.91	0.23	0.31	0.02	49.92	100.00
				Na-Mgs	19.57	1.79	0.05	4.53	23.87	49.91	100.00
$(MgO)_{15}(SiO_2)_{15}(FeO)_{20}Carb^*_{50}$											
H3947-2	1500	60	*L* + *Sti* + $(Wus/Per)_{ss}$	*L*	41.38	4.47	2.11	10.04	9.81	32.20	100.00
				MWus	13.10	85.05	0.44	0.37	0.44	–	99.67
				Sti	0.56	1.95	95.60	0.62	0.25	–	99.34
S6026-1	1350	120	*L* + *Sti* + $(Wus/Per)_{ss}$ + *Carb**	*MWus*	7.43	86.51	0.40	0.31	0.42	–	95.08
				Sti	0.55	1.26	93.04	0.52	0.55	–	95.91
				Mgs	47.67	7.02	0.50	0.69	0.75	43.11	100.00
				Na-Mgs	14.07	1.76	0.06	4.14	24.75	54.33	100.00
$(MgO)_6(SiO_2)_{24}(FeO)_{20}Carb^*_{50}$											
S6028-1	1900	30	*L* + *Sti*	*L*	14.20	33.43	9.30	8.42	8.20	26.46	100.00
				Sti	0.54	0.89	97.53	0.16	0.09	–	99.33
S6027-1	1700	30	*L* + *Sti* + $(Wus/Per)_{ss}$	*L*	24.91	7.29	12.10	12.59	7.10	37.00	100.00
				Sti	0.48	1.20	93.36	0.36	0.35	–	95.76
				MWus	7.40	87.19	0.64	0.32	2.25	–	97.80
H3944-2	900	120	*L* + *Sti* + $(Wus/Per)_{ss}$ + *Carb**	*Sti*	0.14	0.87	93.01	0.20	0.15	–	95.00
				MWus	8.16	87.66	1.18	0.50	0.32	–	97.82
				Mgs	39.46	14.09	0.55	0.67	0.13	45.09	100.00
				Na-Arg	0.27	1.05	0.36	42.51	17.06	38.75	100.00

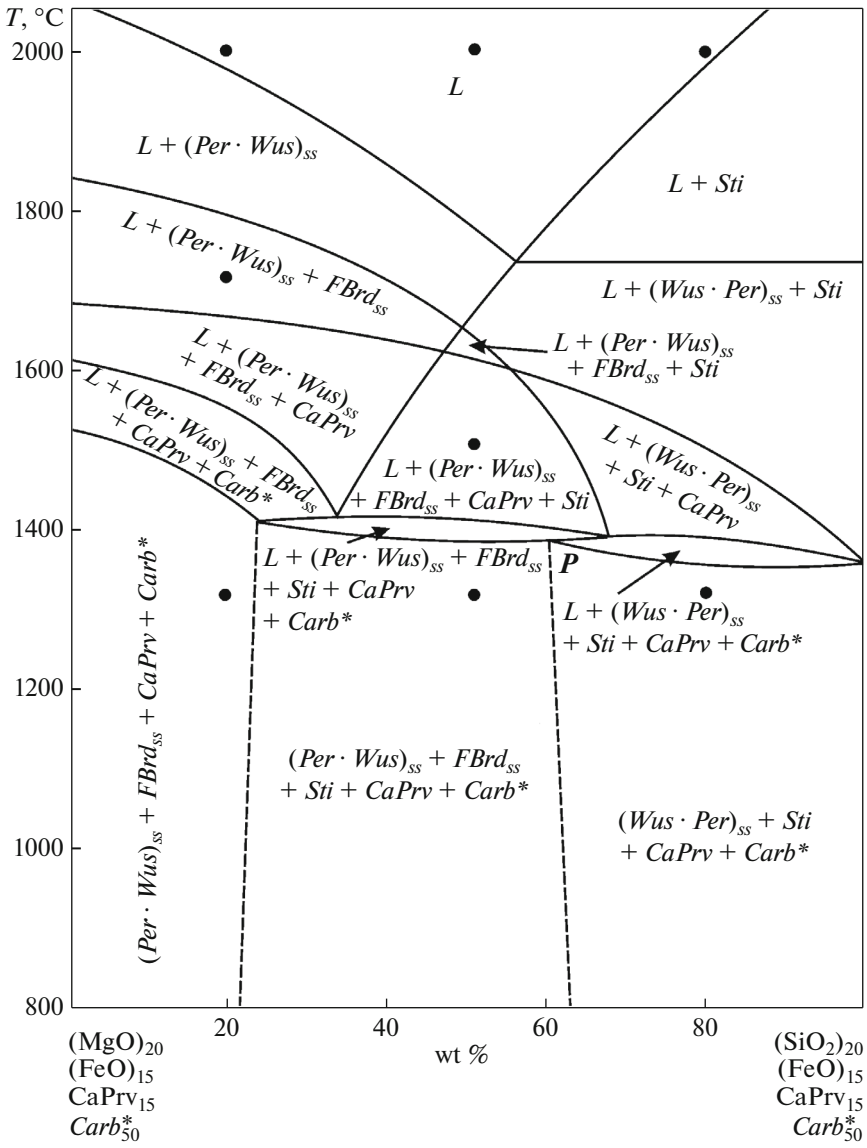

Fig. 6. Melting relations in the polythermal section $(MgO)_{20}(FeO)_{15}CaPrv_{15}Carb^*_{50}$–$(SiO_2)_{20}(FeO)_{15}CaPrv_{15}Carb^*_{50}$ at 26 GPa. *Carb**, simplified abbreviation for carbonates (explained in the text). See Fig. 1 for other mineral symbols.

minerals and their associations (rocks), carbonates, and carbon, since their physicochemical interaction controls the following parameters: (1) variable chemical and phase compositions of melts and solutions parental for diamonds and associated paragenetic minerals; (2) physicochemical causes and mechanisms of nucleation and growth of diamond crystals; (3) physicochemical causes and mechanisms of simultaneous crystallization of diamonds and rock-forming minerals, which provides conditions for growth trapping of primary inclusions in diamonds; and (4) physical and physicochemical conditions of the ultrabasic–basic evolution of diamond-forming melts and solutions in the mode of fractional crystallization and the formation of mineral phases of the ultrabasic and basic parageneses genetically associated with diamonds. In addition, the significance of accessory phases, both paragenetic (they can be solved and crystallize in parental melts) and xenogenic (they are insoluble in parental melts and immiscible with them), becomes clearer. They have a secondary, physicochemically dependent role in the origin of diamonds. Therefore, the accessory mineral phases soluble in parental media, in spite of their belonging to both ultrabasic and basic associations, should be included in the common boundary category (admixture soluble phases) to simplify the diagram; in addition, carbon as the common component of all boundary compositions is removed outside the generalized diagram. A special place in the generalized compositional dia-

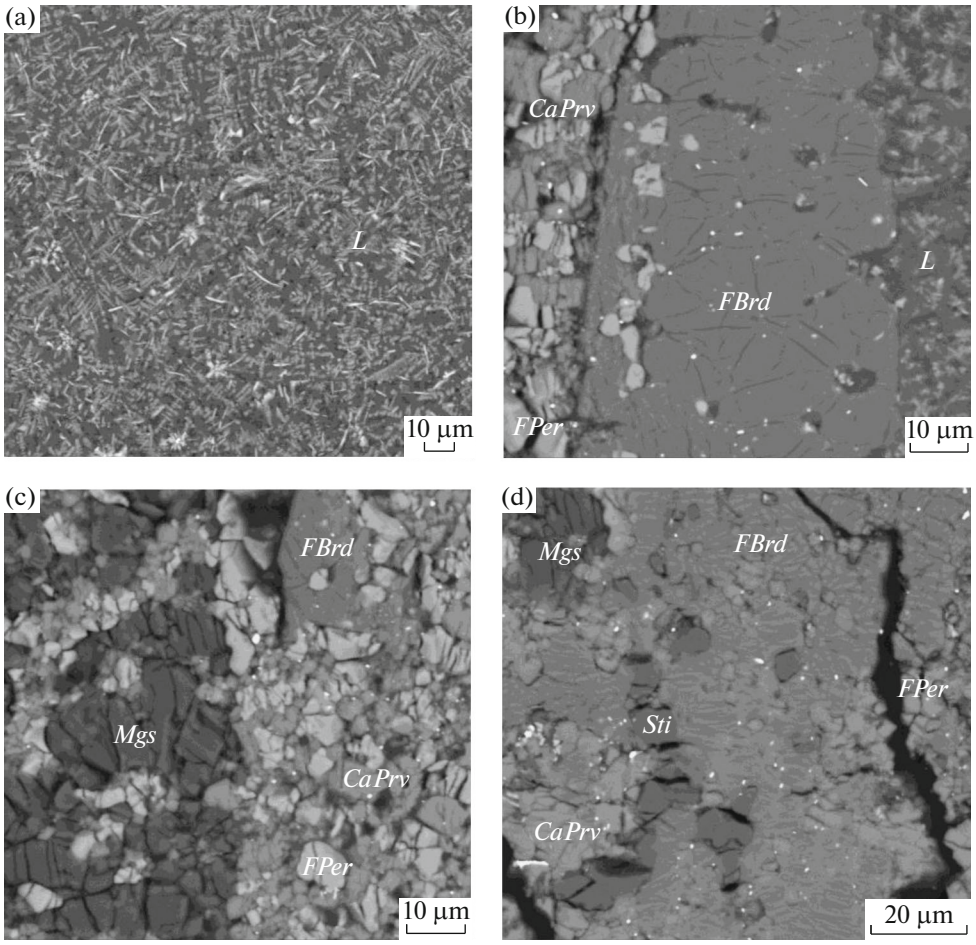

Fig. 7. SEM images of experimental samples in the polythermal section $(MgO)_{20}(FeO)_{15}CaPrv_{15}Carb^{*}_{50}$–$(SiO_2)_{20}(FeO)_{15}CaPrv_{15}Carb^{*}_{50}$ at 26 GPa after quenching. The starting compositions: (a–c) $(MgO)_{16}(FeO)_{15}CaPrv_{15}(SiO2)_4Carb^{*}_{50}$; (d) $(MgO)_{10}(FeO)_{15}$ $CaPrv_{15}(SiO_2)_{10}Carb^{*}_{50}$. *Carb**, simplified abbreviation for carbonates (explained in the text); *FPer*, ferropericlase [= $(Per \cdot Wus)_{ss}$]; *MWus*, magnesiowustite [= $(Wus \cdot Per)_{ss}$]. See Fig. 1 for other mineral symbols.

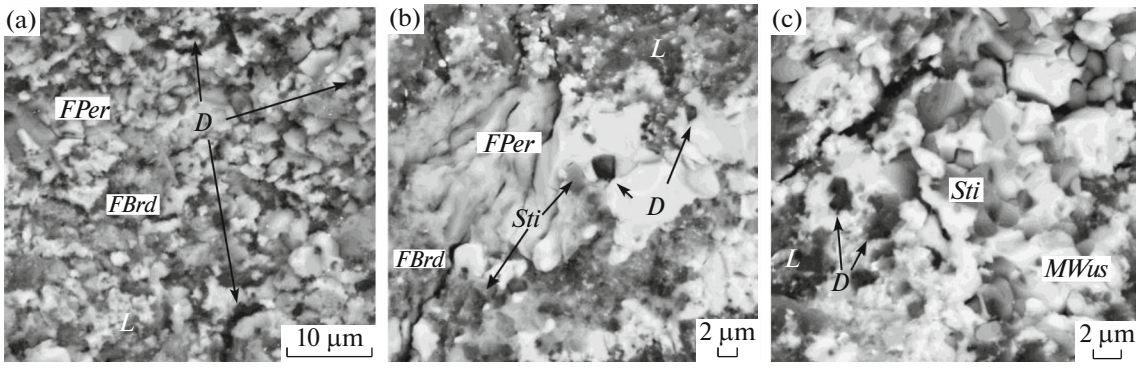

Fig. 8. SEM images of crystallization of diamonds and associated phases in melts and solutions supersaturated with dissolved carbon (graphite) on the basis of the polythermal section $(MgO)_{30}(FeO)_{20}Carb^{*}_{50}$–$(SiO_2)_{30}(FeO)_{20}Carb^{*}_{50}$ (Fig. 4) at 26 GPa after quenching. The diamond-forming starting compositions with graphite are shown in projection on the phase diagram (Fig. 4, black triangles *1–3*. The starting compositions (a) $(MgO)_{12.6}(FeO)_{12}(SiO_2)_{5.4}Carb^{*}_{30}G_{40}$, (b) $(MgO)_9(FeO)_{12}(SiO_2)_9Carb^{*}_{30}G_{40}$, and (c) $(MgO)_{5.4}(FeO)_{12}(SiO_2)_{12.6}Carb^{*}_{30}G_{40}$ correspond to black triangles *1–3* in Fig. 4, respectively. *Carb**, simplified abbreviation for carbonates (explained in the text); *G*, graphite; *D*, diamond. See Fig. 1 for other mineral symbols.

Table 3. Run conditions, compositions of experimental phases, and estimates of the equilibrium mineral associations in the polythermal section $(MgO)_{20}(FeO)_{15}(CaSiO_3)_{15}Carb^*_{50}$–$(SiO_2)_{20}(FeO)_{15}(CaSiO_3)_{15}Carb^*_{50}$ of the original lower-mantle system MgO–FeO–SiO_2–$CaSiO_3$–*Carb** at 26 GPa

Sample	*T*, °C	*t*, min	Experimental results									
			Phase association	Phase	MgO	FeO	SiO_2	CaO	Na_2O	CO_2**	total
					wt %						
$(MgO)_{16}(SiO_2)_4(FeO)_{15}(CaSiO_3)_{15}Carb^*_{50}$											
H4072d	2000	10	*L*	*L*	21.59	23.91	12.49	13.93	6.65	21.43	100.00
H4072d-1	1750	20	*L* + $(Per/Wus)_{ss}$ + *FBrd*	*L*	10.39	12.13	1.98	16.52	8.14	27.25	100.00
				FPer	40.73	53.70	1.62	1.05	2.12	–	99.22
				FBrd	29.89	11.32	54.32	3.87	0.14	–	99.53
H4072d-2	1350	40	$(Per/Wus)_{ss}$ + *FBrd* + *CaPrv* + *Carb**	*MWus*	37.14	59.73	0.40	0.41	1.44	–	99.12
				FBrd	33.60	11.63	53.04	1.54	0.13	–	99.94
				CaPrv	1.12	2.01	49.93	46.36	0.36	–	99.78
				Mgs	47.74	6.63	0.11	0.57	0.05	44.90	100.00
				Ca-Mgs	18.59	11.75	0.36	19.63	7.87	41.80	100.00
$(MgO)_{10}(SiO_2)_{10}(FeO)_{15}(CaSiO_3)_{15}Carb^*_{50}$											
H4073d	2000	10	*L*	*L*	16.45	23.92	19.27	14.25	6.24	19.87	100.00
H4073d-1	1500	20	*L*+ $(Wus/ Per)_{ss}$ + *FBrd* + *Sti* + *CaPrv*	*L*	12.89	10.06	1.02	18.64	12.05	45.34	100.00
				MWus	37.23	60.60	0.24	0.71	1.16	–	99.95
				FBrd	32.46	12.79	53.74	0.6	0.14	–	99.73
				Sti	0.18	0.25	99.36	–	–	–	99.79
				CaPrv	0.95	0.86	51.36	46.81	0.1	–	100.08
H4073d-2	1350	40	$(Wus/Per)_{ss}$ + *FBrd* + *Sti* + *CaPrv* + *Carb**	*MWus*	27.28	69.18	0.18	0.15	3.81	–	99.60
				FBrd	32.19	13.79	53.04	0.71	0.18	–	99.91
				Sti	0.15	0.33	99.08	0.22	-	–	99.79
				CaPrv	0.90	1.29	50.79	46.69	0.27	–	99.93
				Mgs	33.79	7.33	0.26	5.62	4.34	48.66	100.00
				Ca-Mgs	14.92	9.55	0.75	18.09	8.1	48.59	100.00
$(MgO)_4(SiO_2)_{16}(FeO)_{15}(CaSiO_3)_{15}Carb^*_{50}$											
H4074d	2000	10	*L*	*L*	15.72	19.05	25.91	15.95	4.85	18.52	100.00
H4074d-1	1800	20	*L*+ *Sti*	*L*	21.65	19.63	21.35	16.74	4.20	16.43	100.00
				Sti	0.38	0.68	97.77	0.44	–	–	99.25

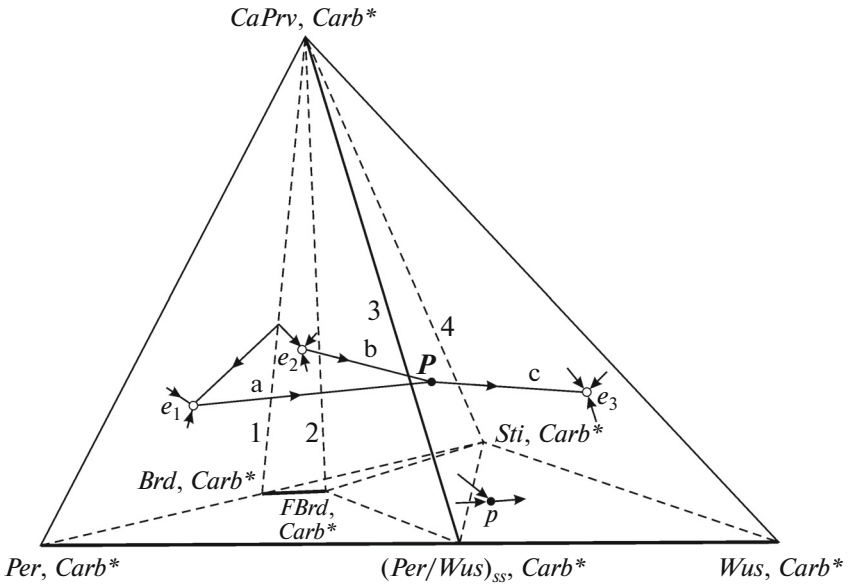

Fig. 9. Liquidus structure of the lower-mantle diamond-forming system *Per–Wus–Sti–CaPrv–Carb** at 26 GPa. *Carb**, simplified abbreviation for carbonates (explained in the text). See Fig. 1 for other mineral symbols. The subsolidus phase triangular volumes are indicated as 1–4; eutectic and peritectic points of triangular boundary systems, as e_1 (L + *Per* + *Brd* + *CaPrv* + *Carb**), e_2 (L + *Brd* + *Sti* + *CaPrv* + *Carb**), e_3 (L + *Sti* + *Wus* + *CaPrv* + *Carb**), and p (L + *Brd* = *Sti* + *MWus* + *Carb**); *P*, quasi-nonvariant peritectic point L + (*FPer* ↔ *MWus*) + *FBrd* + *Sti* + *CaPrv* + *Carb** of the five-component system with the key reaction L + *FBrd* = *Sti* + $(Wus \cdot Per)_{ss}$ + *Carb** (stishovite paradox). The monovariant cotectic curves: (a) ultrabasic L + *FPer* + *FBrd* + *CaPrv* + *Carb**; (b) basic L + *Sti* + *FBrd* + *CaPrv* + *Carb**; (c) basic L + *Sti* + *MWus* + *CaPrv* + *Carb**.

gram is occupied by accessory mineral phases, which are combined in the group of admixture insoluble components.

The generalized diagram of the compositions of parental diamond-forming media under lower-mantle conditions (Fig. 9) is based on the major tetrahedron showing the boundary ultrabasic compositional triangle (*FPer–FBrd–CaPrv*) at the vertices, as well as on the following compositional tetrahedrons: basic (*FBrd–CaPrv–MWus*), carbonate (*Mag–Arg–Sdr–* Na_2CO_3), and that of admixture soluble components (oxides–silicates–other brines–volatiles). The compositional tetrahedron of admixture insoluble components (metals–sulfides–titanates–carbides) is separated by the conventional boundary of complete liquid immiscibility (BCLI). Of key importance is the triangular field on the boundary ultrabasic–basic–carbonate system, which represents the variable chemical and phase compositions of melts and solutions parental for diamonds and associated paragenetic minerals. This field of diamond-forming parental media is located directly near the boundary tetrahedron of carbonates and limited from the top by the line of the crystallization barrier of diamond nucleation (CBDN) determined experimentally. The arrow denoted FC (fractional crystallization) on this line indicates the necessity of the mode of fractional crystallization to realize the ultrabasic–basic evolution of parental media within the field of diamond-forming media.

At the same time, the generalized diagram of the compositions of diamond-forming media (Fig. 11) involves (directly or indirectly) a system of chemical and physicochemical peculiarities, the combination of which controls regularities in the genesis of diamonds and associated phases under lower-mantle conditions. Among such peculiarities are the following. First, the physicochemical nature of the original silicate–oxide material of the lower mantle includes the peritectic reaction between ferrobridgmanite and solidus melts with the formation of stishovite in association with the phases of the periclase–wustite solid solutions (an effect of the stishovite paradox). This peritectic reaction controls the probability of the ultrabasic–basic evolution of original magmas under the mode of fractional crystallization. Second, the formation of primary carbonate melts, which may solve elementary carbon, the component of diamond-forming media, is possible. Such carbonate melts and solutions may be formed in the reactions of metasomatic agents with lower-mantle magmatic rocks. Third, silicate–oxide–carbonate–carbon melt/solutions can be formed upon dissolution of host rocks by primary carbonate melts as parental media with the compositions necessary and sufficient for crystallization of diamonds and genetically associated mineral phases corresponding to the syngenesis criterion. Fourth, the physicochemical nature of the silicate–oxide–carbonate–carbon diamond-forming media of the lower mantle inherits (from the parental material) the peritectic reaction between ferrobridgmanite and solidus carbonate-bearing melts with the formation of stishovite in association with the phases of the periclase–wustite solid

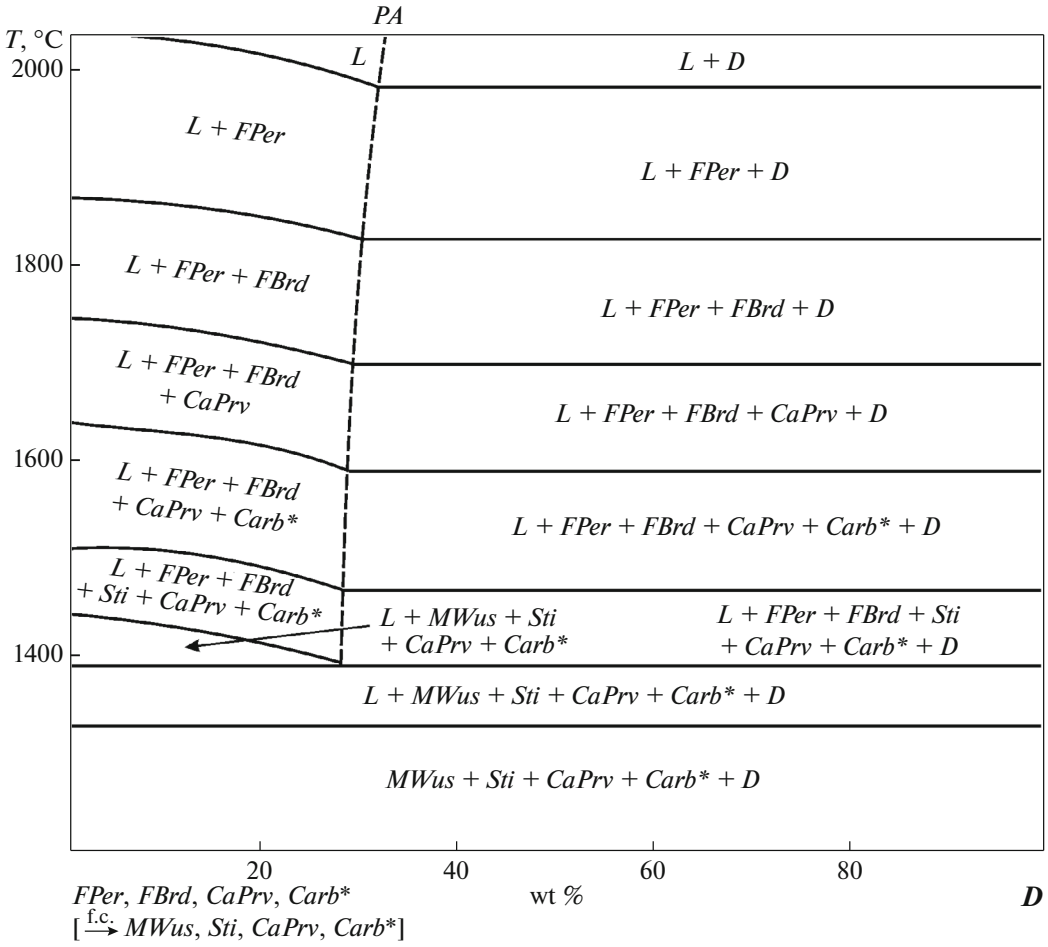

Fig. 10. Diagram of syngenesis of lower-mantle diamonds and minerals of the ultrabasic and basic associations under the conditions of fractional crystallization in the ultrabasic system *FPer–FBrd–CaPrv–Carb*–D* with the final formation of the basic association *MWus* + *Sti* + *CaPrv* + *Carb** + *D*. *Carb**, simplified abbreviation for carbonates (explained in the text); *D*, diamond. See Fig. 1 for other mineral symbols.

solutions (an effect of the stishovite paradox). This peritectic reaction controls the probability of the magmatic ultrabasic–basic evolution of diamond-forming melts in the mode of fractional crystallization. Fifth, accessory admixture mineral phases and components including volatiles are soluble in diamond-forming melts, but their role is minor. Sixth, accessory admixture xenogenic minerals insoluble in diamond-forming melts do not have physicochemical influence on the processes of the formation of diamonds and associated paragenetic phases. Seventh, despite the mineralogical similarity, the chemical and physicochemical conditions of the formation of inclusions of primary paragenetic minerals in diamonds (in parental silicate–oxide–carbonate melts), on the one hand, and minerals of original silicate–oxide rocks of the lower mantle, on the other hand, are fundamentally different.

CONCLUSIONS

According to the mineralogical data, diamonds and primary mineral inclusions in them were formed in a common growth medium under lower-mantle conditions. The key tasks in the study of diamond genesis in the lower mantle are the following: (1) study of the chemical nature and compositions of growth melts for diamonds and paragenetic minerals; (2) understanding of the physicochemical mechanisms of syngenesis of diamonds and primary inclusions; (3) study of the phase reactions responsible for the formation of discrete ultrabasic and basic mineral parageneses in inclusions in lower-mantle diamonds. Lower-mantle diamond-forming melts and solutions belong to the system $(MgO \cdot FeO)_{ss}$–CaO–SiO_2–(Mg–Fe–Ca–Na carbonate)–carbon with the melting relations studied in the physicochemical experiment at 26 GPa. The boundary chemical conditions of the multicomponent diamond-forming system are consistent with the data on the compositions of primary paragenetic inclusions in lower-mantle natural diamonds. The consistent experimental and mineralogical data allow us to suggest silicate–oxide–carbonate melts as the parental media for diamonds and associated phases in the lower mantle. Achievement of the supersaturated

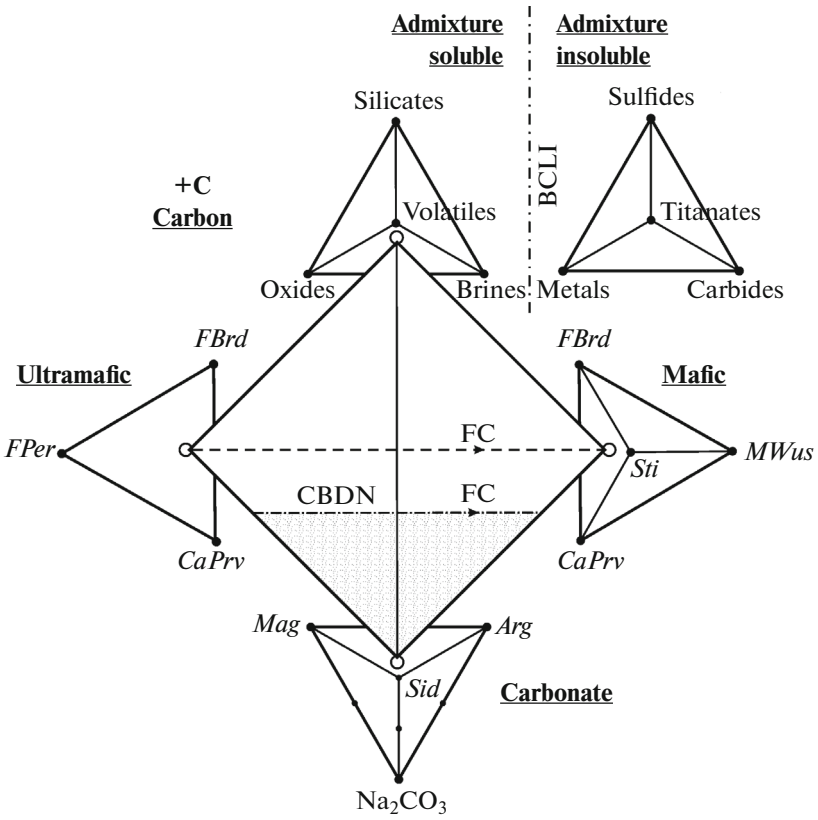

Fig. 11. Generalized compositional diagram for lower-mantle melts and solutions parental for diamonds and associated minerals (including primary inclusions). *Mag*, magnesite, *Arg*, aragonite; *Sid*, siderite. See Fig. 1 for other mineral symbols. CBDN, concentration barrier of diamond nucleation; FC, fractional crystallization; BCLI, conventional boundary of complete liquid immiscibility.

state of dissolved carbon in relation to diamond in completely miscible silicate–oxide–carbonate melts provides the physicochemical mechanism responsible for nucleation and mass crystallization of diamonds. Growth of diamond crystals is accompanied by the formation of paragenetic mineral phases in common growth media. In addition, the fractional ultrabasic–basic evolution of diamond-forming melts occurs. Such chemically contrasting evolution becomes possible due to the peritectic reaction between ferrobridgmanite $(Mg,Fe)SiO_3$ and carbonate-bearing melt with the formation of the phases of periclase–wustite complete solid solutions $(MgO/FeO)_{ss}$ and stishovite SiO_2 (the mechanism of the stishovite paradox). This mechanism is observed in the original lower-mantle systems free of the carbonate components as well. The evolution is accompanied by the successive paragenetic transition from the ultrabasic ferropericlase- and ferrobridgmanite-bearing associations to the basic magnesiowustite- and stishovite-bearing associations in the original lower mantle silicate–oxide, as well as in the diamond-forming silicate–oxide–carbonate systems. Based on the experimental and mineralogical data, we developed the mantle carbonatite theory of the origin of lower-mantle diamonds and suggested the genetic classification of mineral inclusions in them.

ACKNOWLEDGMENTS

The authors are grateful to Professor L.S. Dubrovinsky for providing facilities and methodological help in high-pressure multianvil experiments at the Bayerisches Geoinstitute, University of Bayreuth, Germany. This study was supported by the Presidium of the Russian Academy of Sciences (program no. I.P.08), the Russian Foundation for Basic Research (project no. 16-05-00850), and the Foundation of the President of the Russian Federation (project MD-3464.3017.5).

REFERENCES

M. Akaogi, "Phase transformations of minerals in the transition zone and upper part of the lower mantle," *Advances in High-Pressure Mineralogy,* Ed. by E. Ohtani, Geol. Soc. Am. Spec. Pap. 421, 1–13 (2007).

G. P. Bulanova, M. J. Walter, C. B. Smith, S. C. Kohn, L. S. Armstrong, J. Blundy, and L. Gobbo, "Mineral inclusions of sublithospheric diamonds from Collier 4 kimberlite pipe, Juina, Brazil: subducted protoliths, carbonated melts, and primary kimberlite magma-

tism," Contrib. Mineral. Petrol. **159** (4), 489–510 (2010).

D. J. Frost, B. T. Poe, R. G. Tronnes, C. Libske, F. Duba, and D. C. Rubie, "A new large-volume multianvil system," Phys. Earth Planet. Inter. **143**, 507–514 (2004).

B. Harte and L. W. Harris, "Lower mantle mineral association preserved in diamonds," Mineral. Mag. **58A**, 384–385 (1994).

T. Irifune and T. Tsuchiya, "Mineralogy of the Earth – phase transitions and mineralogy of the lower mantle," *Treatise on Geophysics* (Elsevier, 2007), pp. 33–62.

F. Kaminsky, "Mineralogy of the lower mantle: a review of 'super-deep' mineral inclusions in diamond," Earth Sci. Rev. **110**, 127–147 (2012).

F. V. Kaminsky, O. D. Zakharchenko, W. L. Griffin, D. M. Channer, and G. K. Khachatryan-Blinova, "Diamond from the Guaniamo area, Venezuela," Can. Mineral. **38**, 1347–1370 (2000).

F. V. Kaminsky, G. K. Khachatryan, P. Andreazza, D. Araujo, and W. I. Griffin, "Super-deep diamonds from kimberlites in the Juina area, Mato Crosso State, Brazil," Lithos **112S**,(2), 833–842 (2009).

Yu. A. Litvin, "Hot mantle spots and experiment up to 10 GPa: alkaline reactions, carbonatization of lithosphere, and new diamond-forming systems," Russ. Geol. Geophys. **39** (12), 1772–1779(1998).

Yu. A. Litvin, "High pressure mineralogy of diamond genesis," *Advances in High-Pressure Mineralogy,* Ed. by E. Ohtani, Geol. Soc. Amer. Spec. Pap. **421**, 83–103 (2007).

Yu. A. Litvin, "The stishovite paradox in the genesis of superdeep diamonds," Dokl. Earth Sci. **455**, 274–278 (2014).

Yu. A. Litvin, *Genesis of Diamonds and Associated Phases* (Springer, 2017).

Yu. Litvin, A. Spivak, N. Solopova, and L. Dubrovinsky, " On origin of lower-mantle diamonds and their primary inclusions," Phys. Earth Planet. Inter. **228**, 176–185 (2014).

Yu. A. Litvin, A. V. Spivak, and L. S. Dubrovinsky, "Magmatic evolution of the Earth's lower mantle: stishovite paradox and origin of superdeep diamonds (experiments at 24–26 GPa)," Geochem. Int. **54** (11), 936–947 (2016a).

Yu. A. Litvin, A. V. Spivak, A. Simonova, and L. S. Dubrovinsky, "On origin and evolution of diamond-forming lower-mantle systems: physicochemical studies in experiments at 24 and 26 GPa," J. Phys. Conf. Ser. (JPCS) – IOP Conference Series (2016b).

Yu. A. Litvin, A. V. Spivak, and A. V. Kuzyura, "Fundamentals of mantle carbonatite concept of diamond genesis," Geochem. Int. **54** (10), 839–857 (2016c).

Yu. A. Litvin, A. V. Spivak, and L. S. Dubrovinsky, "Origin of lower-mantle diamonds and associated minerals," *High Pressure Science and Technology, 54th EHPRG-54 Meeting, Bayreuth, Germany, 2016* (Bayreuth, 2016a) abstracts: MS15-O15.6. www.ehprg 2016.org, p. 291.

Yu. A. Litvin, A. V. Spivak, D. A. Simonova, and L. S. Dubrovinsky, "The stishovite paradox in the evolution of lower mantle mamas and diamond-forming melts (Experiment at 24 and 26 GPa)," Dokl. Earth Sci. **473**, 444–448 (2017).

L. S. Palatnik and A. I. Landau, *Phase Equilibria in Multicomponent Systems* (Holt, Rinehart and Winston, Inc., New York, 1964).

F. N. Rhines, *Phase Diagrams in Metallurgy. Their Development and Application* (McGraw-Hill Company, New York–Toronto–London, 1956).

A. E. Ringwood, *Composition and Petrology of the Earth's Mantle.* (McGraw-Hill, New York–Toronto, 1975).

M. Schrauder and O. Navon, "Hydrous and carbonatitic mantle fluids in fibrous diamonds from Jwaneng, Botswana," Geochim. Cosmochim. Acta **52**, 761–771 (1994).

B. N. Scott Smith, R. V. Danchin, J. W. Harris, and K. J. Stracke, "Kimberlites near Orroroo, South Australia. Kimberlites I," *Kimberlites and Related Rocks*, Ed. by L. Cornprobst (Elsevier, Amsterdam, 1984), pp. 121–142.

S. Yu. Skuzovatov, D. A. Zedgenizov, A. L. Ragozin, and V. S. Shatsky, "Growth medium composition of coated diamonds from the Sytykanskaya kimberlite pipe (Yakutia)," Russ. Geol. Geophys. **53** (11), 1197–1208 (2012).

A. Spivak, N. Solopova, L. Dubrovinsky, and Yu. Litvin, "Melting relations of multicomponent carbonate $MgCO_2$–$FeCO_3$–$CaCO_3$–Na_2CO_3 system at 11–26 GPa: application to deeper mantle diamond formation," Phys. Chem. Miner. **42**, 817–824 (2015).

A. M. Zakharov, *Phase Diagrams of Four-Component Systems* (Metallurgiya, Moscow, 1964) [in Russian].

D. A. Zedgenizov, A. L. Ragozin, V. S. Shatsky, D. Araujo, and W. L. Griffin, "Fibrous diamonds from the placers of the northeast Siberian Craton: carbonate and silicate crystallization media," Russ. Geol. Geophys. **52** (11), 1286–1297.

Translated by A. Bobrov